Relaxation of Ultrathin Polystyrene Films Hyperswollen in Supercritical Carbon Dioxide

ARTICLE *in* MACROMOLECULES · DECEMBER 2014

Impact Factor: 5.8 · DOI: 10.1021/ma501281t

Macromolecules

Article

pubs.acs.org/Macromolecules

Relaxation of Ultrathin Polystyrene Films Hyperswollen in Supercritical Carbon Dioxide

J. K. Bal,*[,†,§] T. Beuvier,[†] M. S. Chebil,[†,‡] G. Vignaud,[‡] Y. Grohens,[‡] M. K. Sanyal,[⊥] and A. Gibaud*[,†]

[†]LUNAM Université, IMMM, Faculté de Sciences, Université du Maine, UMR 6283 CNRS, Le Mans Cedex 9, 72000, France

[§]Centre for Research in Nanoscience and Nanotechnology, University of Calcutta, Technology Campus, Block JD2, Sector III, Saltlake City, Kolkata, 700098, India

[‡]Laboratoire d'Ingénierie des MATériaux de Bretagne, Centre de Recherche, Rue de Saint Maudé, BP 92116, 56321 Lorient Cedex France

[⊥]Surface Physics and Material Science Division, Saha Institute of Nuclear Physics, 1/AF Bidhannagar, Kolkata 700064, India

Supporting Information

ABSTRACT: Relaxation of highly swollen (~20−80%) ultrathin (≤21 nm) polystyrene films exposed to supercritical carbon dioxide (at 35 °C and 80 bar) is studied by monitoring the evolution of thickness as a function of time using X-ray reflectivity. Correlations between their swelling (that determines the departure from equilibrium), depressurization time, thickness relaxation rate and aging time are established. Swollen films that are depressurized very slowly (depressurization time ≈1 h) exhibit a small swelling and a very low relaxation rate at ambient condition, whereas fast depressurized films (depressurization time ≈2 min) show a large swelling and a high relaxation rate. The rate of depressurization not only impacts their out of equilibrium state but also their relaxation rate. The relaxation time is essentially governed by the temperature following an Arrhenius law below T_g and a strong temperature-dependent behavior above T_g and by the relative departure from equilibrium.

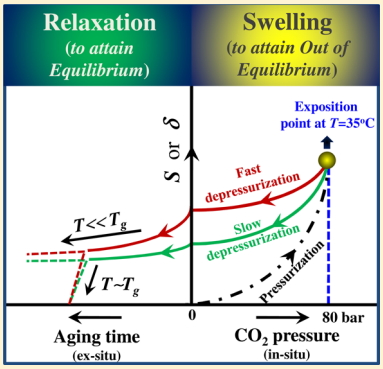

INTRODUCTION

Over the last 2 decades, the use of supercritical fluids such as carbon dioxide (CO_2) has emerged as a leading alternative to toxic organic solvents in polymer processing and synthesis, reactor clean up and preparation of pharmaceutical products.[1−8] CO_2 is well-known as an abundant, nontoxic, inexpensive and inflammable substance. Furthermore, its critical temperature is 31 °C,[9] which is not far from the room temperature and its solvent quality can be well tuned with small variations in pressure and/or temperature.[5] The tunable properties of supercritical carbon dioxide ($scCO_2$) make it of paramount importance for manipulating and controlling the interfacial, thermodynamic and transport properties of polymer thin films.[7]

While the effect of CO_2 has been studied extensively in thick films since long back and more recently in thin films,[10−32] it has been far less investigated for ultrathin films (especially for thickness ≤20 nm).[26,27,33] An anomalous behavior with enhanced swelling is experienced in ultrathin films unlike to bulk in the vicinity of the critical point of CO_2. In this region CO_2 is highly compressible and CO_2 exhibits important density fluctuations along a ridge. Koga et al.[20] justified this anomalous swelling behavior by enhanced solubility of CO_2 whereas Sirad et al.[21] explained it by the phase separation of CO_2-rich and polymer-rich domains within the films. On the other hand the properties exhibited by thin polymer films are substantially different from those of bulk films due to the change in confinement which modifies the polymer chain conformations and mobility near interfaces.[34−36] In thin films, Frank et al.[37] reported that the mobility or lateral diffusion coefficient of polymer can be influenced by the substrate and interfacial effects. Keddie et al.[34] evidenced thickness dependent glass transition temperatures (T_g) for polystyrene (PS) and poly(methyl methacrylate) (PMMA) films using ellipsometry technique. Koga et al.[24] have shown by neutron reflectivity that the swellability of PS and polybutadiene (PB) films exposed to $scCO_2$ is bigger for thinner films. Theoretical studies predict that the large compressibility of supercritical fluids can also affect the swelling behavior of polymer thin films.[38−40] Many efforts have been devoted to investigate the swelling behavior of cross-linked[11,41] and uncross-linked[42] poly(dimethylsiloxane) (PDMS) bulk and thin films. Using surface plasmon resonance (SPR) technique, Fishburn reported the in situ adsorption of PDMS to $scCO_2$.[43] In this respect, X-ray reflectivity (XRR) technique is rarely used. This technique is nevertheless the most suitable technique to measure the thickness of less than 200 nm thick films with a very high precision (~an angstrom) due to the wide range of accessible q_z wave vector transfer and high dynamical range of X-ray instruments. Furthermore, quantitative analysis of XRR data

Received: June 21, 2014
Revised: October 4, 2014

   dx.doi.org/10.1021/ma501281t | Macromolecules XXXX, XXX, XXX−XXX

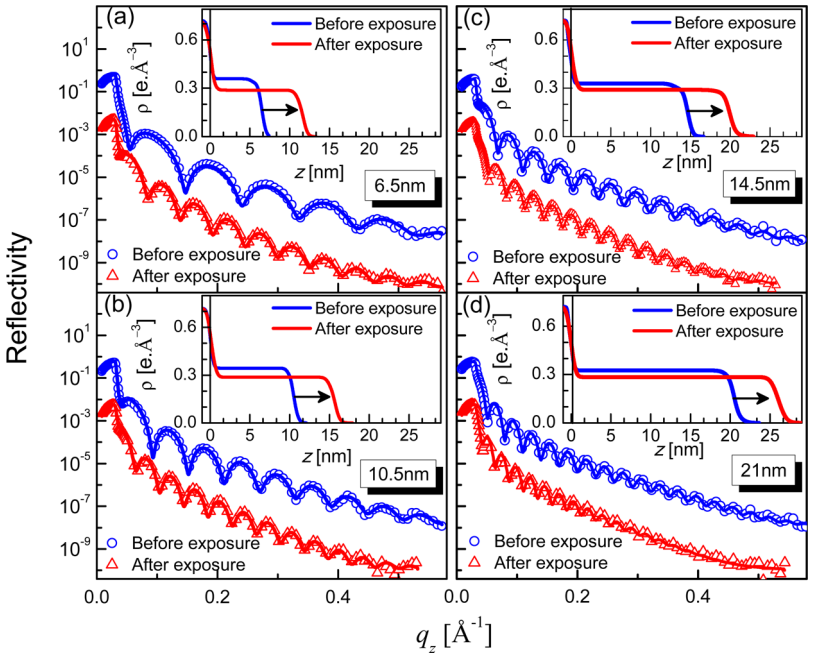

Figure 1. XRR data (different symbols) and analyzed curves (solid line) of (a) 6.5, (b) 10.5, (c) 14.5, and (d) 21 nm PS films before and after $scCO_2$ exposure with fast depressurization (within 2 min). The curves are shifted vertically for clarity. Insets: corresponding EDPs. Arrows indicate the swelling of the films. All the samples were depressurized within 2 min and characterized by XRR within few hours at ambient conditions.

yields the electron density profile (EDP) in the direction normal to the surface of the film.[44,45] It is then feasible to determine the amount of adsorbed or trapped CO_2 within the swollen polymer films as it was shown in our previous study[33] although large errors in this amount can be easily made.[46] In addition to measuring the thickness of thin films with a very high precision, XRR can also be used to follow the thickness relaxation of swollen films that are clearly in a nonequilibrium state.

Below T_g, polymers are in a nonequilibrium glassy state that is intrinsically unstable. Resulting sluggishness of arrested structures hinders equilibration. Hence they undergo structural relaxation over logarithmic time scale known as physical aging. While the physical aging of bulk and thick (>100 nm) glassy polymers is well understood, the aging of ultrathin films (≤20 nm) has been far less studied. The effect of the temperature and solvent quenching have been investigated especially on PS[47,48] and PMMA[49] thin films. Within these two studies, the relaxation rate β, defined as the change in thickness per unit time, was found to be proportional to the swellability δ. The swellability or relative departure from equilibrium δ that is defined as the ratio between the increment in film thickness over the initial equilibrium film thickness was limited to ∼10%.[49] On the contrary, the exposure to $scCO_2$ has shown high $\delta \sim 43\%$.[33] In particular, exposure under $scCO_2$ causes plasticization which is thought to increase the free volume and to facilitate molecular motions[50,51] that may influence their physical aging characteristics. Surprisingly, literature dealing with physical aging of swollen polymer ultrathin films under $scCO_2$ is not available to the best of our knowledge although Oka et al.[52] reported the free volume-relaxation behavior of highly thick (∼1 mm) PS films swollen under $scCO_2$. Although the swelling under $scCO_2$ has been well studied, physical aging or relaxation of swollen films was rather neglected. Especially, the role of depressurization rate, initial thickness and temperature in the context of physical aging of $scCO_2$-induced swollen PS ultrathin films still remains untouched.

In this work, we demonstrate that the swelling and physical aging of PS ultrathin films exposed to $scCO_2$ are interrelated and can be tuned via the speed of the depressurization. XRR is used to track the evolution of swollen films thickness and structure as a function of aging time at different temperatures.

EXPERIMENTAL SECTION

PS ultrathin films (Polymer Source M_w = 136k) of different thicknesses (varied from 6.5 to 21 nm) were prepared by adjusting the concentration of PS-toluene solutions. Films were deposited by spin coating (Karl Suss) these solutions at 2000 rpm for 1 min onto hydrophilic RCA-treated Si(100) substrates. Werner Kern developed the basic procedure in 1965 while working for RCA (Radio Corporation of America)—hence the name. Details of the RCA treatment were described elsewhere.[46] In brief, the Si surfaces (of size ≈18 × 18 mm^2) were made hydrophilic by immersing them in a mixed solution of ammonium hydroxide (NH_4OH, Sigma-Aldrich, 25%), hydrogen peroxide (H_2O_2, Acros Organics, 35%), and Milli-Q water (H_2O:NH_4OH:H_2O_2 = 2:1:1, by volume) for 10 min at 100 °C. Then the substrates were dried prior to do spin coating. The XRR technique was used to characterize the thickness and quality of the spin coated films that are further designated by their initial thickness.

The samples were then loaded into a pressure cell (SEPAREX Equipment) having a volume of 60 mL. In order to make sure that no impurity or air was present in the cell, we purged the cell two or three times with CO_2 gas at ∼5 bar. We subsequently sealed and pressurized the cell with CO_2 (Air Liquide, N45) using a manual pressure generator (SEPAREX). The cell was heated to the desired temperature using a serpentine in which water was flowing at a fixed and controlled temperature with a precision of ±0.1 °C. The pressure was measured with a precision of ±0.6%. Pressure and temperature were kept fixed to 80 bar and 35 °C, respectively. The cell was depressurized by opening a valve in the cell after 1 h exposition of the samples in $scCO_2$. The rate of depressurization (fast or slow) is controlled by the opening of this valve manually.

XRR measurements were carried out using a versatile X-ray diffractometer (XRD) setup to investigate the structure of PS films.

dx.doi.org/10.1021/ma501281t | Macromolecules XXXX, XXX, XXX−XXX

Table 1. Parameters Obtained from the Analysis of the X-ray Reflectivity Data: Thickness (error ≈ ±0.1 nm) and Volume Electron Density before and after scCO$_2$ Exposure

thickness (nm)		volume density ρ (e$^-$/Å^3) of the film			
			final		
initial	final	initial	film	polymer only	CO$_2$ only
6.5	11.6	0.359 ± 0.032	0.286 ± 0.026	0.201 ± 0.018	0.085 ± 0.044
10.5	15.5	0.343 ± 0.031	0.287 ± 0.026	0.232 ± 0.021	0.055 ± 0.047
14.5	19.7	0.327 ± 0.029	0.287 ± 0.026	0.241 ± 0.022	0.046 ± 0.048
21.0	26.2	0.324 ± 0.029	0.284 ± 0.025	0.261 ± 0.023	0.023 ± 0.048
6.8 (slow)	9.2	0.352 ± 0.032	0.286 ± 0.026	0.260 ± 0.023	0.026 ± 0.049

The diffractometer (Empyrean Panalytical) was equipped with a Cu source (sealed tube) followed by a W/C mirror to select and enhance Cu Kα radiation (λ = 1.542 Å). All measurements were carried out in θ–θ geometry for which the sample was kept fixed during the measurements. The intensity was measured with a Pixel 3D detector using a fixed aperture of 3 channels (0.165°) in the 2θ direction. Under such conditions, at a given angle of incidence θ, a nonvanishing wave vector component, q_z, is given by $(4\pi/\lambda)\sin\theta$ with resolution 0.0014 Å^{-1}. XRR technique essentially provides an EDP, i.e., the average electron density (ρ) in-plane (x–y) as a function of depth (z).[44−46] From the EDP, it is possible to estimate the film thickness, its electron density, and the interfacial roughness. Analysis of XRR data has been carried out using the matrix technique.[44] For the analysis, the film is divided into a number of layers including roughness at each interface.

RESULTS AND DISCUSSION

Swelling. Observed and calculated XRR data before and after scCO$_2$ exposure for films having different thicknesses are shown in Figure 1. For data collected after scCO$_2$ exposure, the experimental conditions were 1 h of CO$_2$ exposure at 80 bar and 35 °C, and a fast depressurization of the cell from 80 bar to atmospheric pressure within 2 min. It is clear in this figure that the films exposed to scCO$_2$ exhibit homogeneous Kiessig fringes having a shorter period than the unexposed ones which proves that a large uniform swelling in out-of-plane direction is retained after depressurization. To obtain EDPs, which contain detailed quantitative information about the film structure, all the reflectivity curves were analyzed. It is obvious that all films are significantly swollen as indicated by arrows in the EDPs shown in the insets of Figure 1.

To characterize the remnant effect of CO$_2$ exposure to the films, the swellability S is defined as the relative change in thickness, i.e., $S = (H_f - H_i)/H_i$, where H_i and H_f indicate the thicknesses of the film before and after CO$_2$ exposure, respectively. From the XRR analysis, we find that the thickness of the 6.5, 10.5, 14.5, and 21.0 nm thick films increases to 11.6, 15.5, 19.7, and 26.2 nm, respectively after exposition yielding a swellability S (%) equal to 78 ± 3%, 48 ± 2%, 36 ± 1% and 25 ± 1%. From the quantitative analysis of the XRR curves it is possible to determine the electron density of the films before and after CO$_2$ exposure. The final electron density (ρ_f) can be separated into two terms. The first one corresponds to the contribution of the polymer only (ρ_f^{PS}) while the second one arises from the contribution of CO$_2$ inside the film ($\rho_f^{CO_2}$). The electronic density can be thus expressed as

$$\rho_f = \rho_f^{PS} + \rho_f^{CO_2} \quad \text{and} \quad \rho_f^{PS} = \rho_i \times H_i/H_f$$

where subscripts "i" and "f" mean before and after CO$_2$ exposure, respectively. Superscripts "PS" and "CO_2" represent the contribution of polystyrene and CO$_2$, respectively.

The decrement of ρ_i after CO$_2$ exposure can be correlated to the enhanced free volume and to the formation of new holes arising from the reorganization of polymer chains. Different techniques, such as, small-angle X-ray scattering (SAXS) and positron annihilation spectroscopy (PAS) have been used to estimate free volume size in polymer. SAXS gives a free volume size distribution whereas PAS provides an average free volume size of the cavity. Chen et al.[53] reported PAS measurements up to 55 bar at room temperature on PS bulk (1 mm thickness). Before CO$_2$ exposure, the hole diameter was estimated to be ≈0.58 nm. This value is quite similar to those found by Oka et al.[52] on bulk PS and by Ata et al.[54] who reported a hole diameter in the 0.58–0.63 nm range depending of the film thickness. After CO$_2$ exposure, it was found that the swelling of PS films in the CO$_2$ gas state is governed mainly via free-volume hole expansion and new holes formation. For instance, Chen et al.[53] reported that on the rise of pressure from 1 to 55 bar, the size of the nano holes increases from 0.55 to 0.68 nm. They also observed that a portion of the free volume remained permanently at room temperature in the polymer after depressurization. In our investigations, we reach the supercritical state of CO$_2$ and more precisely the ridge where critical fluctuations of CO$_2$ density are at the highest.[55,56] Consequently, at this location the swelling is higher than in the gas or the supercritical state away from the ridge. When PS films are exposed at the ridge, we evidence that after depressurization they remain partly swollen. They exhibit a lower electron density than the one of the initial films which is a clear signature of the increase of their free volume fraction.

In addition, we have found that the total amount of electrons in the film is not conserved before and after scCO$_2$ exposure. The amount of electrons increases as evidenced in our previous study.[33] To explain this increment, we assume that the free volume of the polymer is filled by CO$_2$ molecules ($\rho_f^{CO_2} > 0$). Recently, Oka et al.[52] have observed that the weight of bulk PS after scCO$_2$ exposure and depressurization was higher than the initial one. They attributed this difference to the presence of CO$_2$ within the polymer matrix. However, in ultrathin films, the quantity of trapped CO$_2$ is very small and this yields a large uncertainty in this value (given in Table 1). Prior to obtain more averaged information throughout the film, we have also extracted the surface electron density of trapped CO$_2$ from the excess density that comes out 10.7 ± 6, 10.6 ± 8, 9.3 ± 11, and 8.8 ± 15 e$^-$/Å^2 for 6.5, 10.5, 14.5, and 21 nm thick films, respectively. Thus, the trapped amount is comparable to the estimated error and hence it is hard to make any strong comments regarding the trapping of CO$_2$ due to exposure except for the fact that a clear trend was observed. As there is a strong thickness dependency in S, it is worth comparing films of similar thicknesses in order to consider the role of depressurization rate. Figure 2 shows the swelling of another

dx.doi.org/10.1021/ma501281t | Macromolecules XXXX, XXX, XXX–XXX

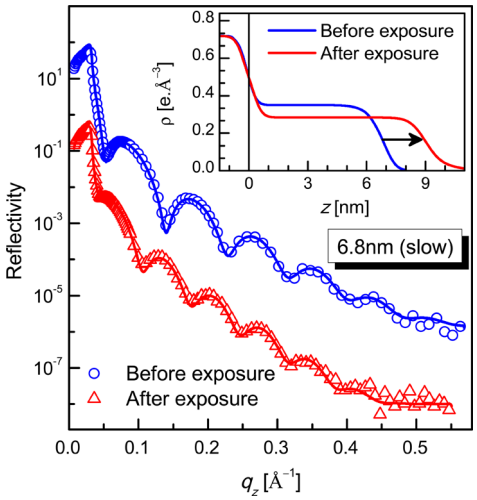

Figure 2. XRR data (different symbols) and analyzed curves (solid line) of 6.8 nm PS film, which is depressurized slowly, before and after $scCO_2$ exposure (curves are shifted vertically for clarity). Inset: corresponding EDPs. This sample was depressurized within 1 h and characterized by XRR within few hours at ambient conditions.

6.8 nm thick film for which the depressurization was carried out very slowly, i.e., within 1 h. Interestingly we observed that S_{slow} ≈ 35 ± 3% was smaller than S_{fast} (≈78 ± 3%) of similar thickness (shown in Figure 1a).

Notably, we have previously[33] shown by in situ XRR measurements of a 7 nm thick PS film grown on a hydrofluoric (HF) acid etched hydrophobic Si substrate that S decreased from >130% at 65 bar to 43% at 0 bar during the depressurization with a hysteresis between the pressurization and depressurization cycles. It should be mentioned that, in this previous study, the rate of depressurization was quite slow as XRR curves were measured at each pressure during depressurization. Interestingly, S ≈ 43% is much less than S ≈ 78% obtained for the fast depressurized 6.5 nm film grown on hydrophilic RCA-treated Si. This tends to show that it is the rate of depressurization which is of primarily importance in the value of S and not the hydrophilicity/hydrophobicity of the substrate. For comparison, we have studied the swelling and evolution of similarly thick PS films grown on both HF- and RCA-treated substrates keeping the depressurization time constant (see Supporting Information, Figure S1). No fundamental differences were observed. Therefore, the large difference in S cannot be attributed to the hydrophobic (HF-

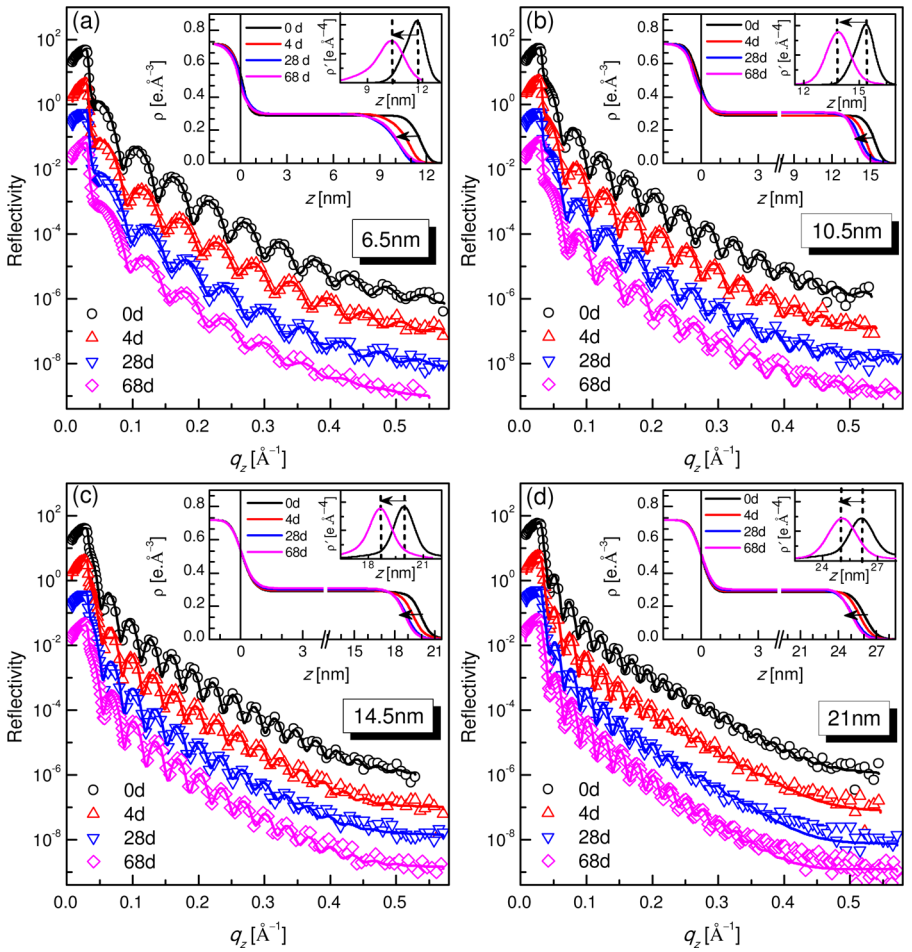

Figure 3. Time evolution XRR data (different symbols) and analyzed curves (solid line) of (a) 6.5, (b) 10.5, (c) 14.5, and (d) 21 nm PS films after fast depressurization under $scCO_2$ exposure (curves are shifted vertically for clarity). d indicates time in day scale. Insets: corresponding EDPs and their (0 and 68 days) derivatives. Positions of two Gaussian peaks (shown by dashed lines) obtained from the derivative of EDPs determines the thickness of the swollen film after 0 and 68 days of depressurization. Relaxation is indicated by arrows. For clarity, we break the z scale in such a way that the z range becomes same for all these four films.

dx.doi.org/10.1021/ma501281t | *Macromolecules* XXXX, XXX, XXX–XXX

treated Si) or hydrophilic (RCA-treated Si) nature of the underlying substrate. Hence in summary, the faster the depressurization rate, the more the film is swollen after depressurization. The next section is now dedicated to the study of the physical aging of these differently swollen films.

Relaxation. *Experimental Evidence for the Relaxation.* Structural relaxation, which is also referred as physical aging, defines the process by which a glass slowly moves back toward equilibrium at a given temperature as a function of time.[57] To study this process, we now present the thickness evolution of swollen films as a function of time at room temperature as well as at elevated temperatures after that films were put outside the pressure cell. The time-evolutions of the XRR profiles and corresponding EDPs along with derivatives for fast depressurized swollen films are shown in Figure 3. There is a clear shift of the Kiessig fringes toward higher q_z values for all films with aging time which is an indication of the decrease of the film thickness. This is also visible in the EDPs and clearer in their derivatives (indicated by arrows). However, this trend has a tendency to level off with time. Notably a slight increment in electron density is found to be associated with the thinning of all the films, suggesting the reduction of the free volume of swollen films. XRR data and EDPs along with their corresponding derivatives at a few days interval for slow depressurized film are shown in Figure 4. In contrary to the

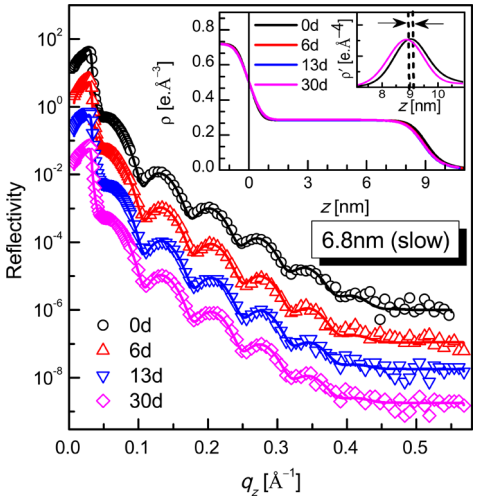

Figure 4. Time evolution XRR data (different symbols) and analyzed curves (solid line) of 6.8 nm PS film (curves are shifted vertically for clarity). d indicates time in day scale. Insets: corresponding EDPs and their (0d and 30d) derivatives. Position of two Gaussian peaks obtained from the derivative of EDPs indicates the thickness of the swollen film after 0 and 30 days of depressurization. Negligible relaxation is indicated by arrows.

films obtained after fast depressurization, the decrement in thickness characteristic of the relaxation is very small. This observation clearly evidences that films are less perturbed or close to equilibrium when the rate of depressurization is slow. However, regardless of the depressurization rate, all films show long-term aging behavior at room temperature.

Analysis of the Relaxation. *At Room Temperature.* To quantitatively understand the relaxation mechanism at room temperature and high temperatures (HT), the thickness of swollen films $H_f(t)$ after a given aging time t at a given temperature T was monitored. The relative departure from the equilibrium thickness δ, is then defined as[49]

$$\delta(t) = \left(\frac{H_f(t) - H_\infty}{H_\infty}\right) = \frac{\Delta H(t)}{H_\infty} \quad (1)$$

where H_∞ is the equilibrium thickness ($\approx H_i$, i.e., the thickness before exposure) at T and departure $\Delta H(t) = H_f(t) - H_i$. Nevertheless, here δ is equivalent to S. We have plotted $\delta_{RT}(t)$ as a function of the logarithm of aging time t for the films of different thicknesses at room temperature in Figure 5. The

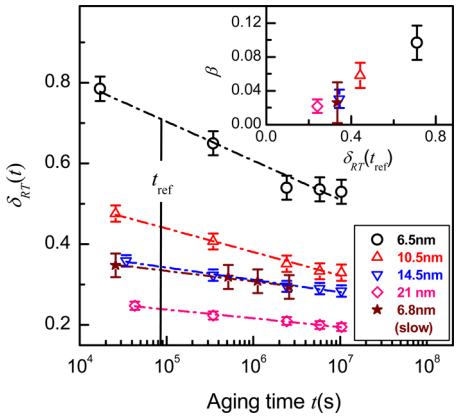

Figure 5. $\delta_{RT}(t)$ of fast depressurized films having different thickness (open symbols) and slow depressurized film (solid symbol) as a function of logarithmic time (t). Dash-dot lines through $\delta_{RT}(t)$ data are slopes of the curves. t_{ref} (=1 day) (solid line) is the selected reference time at which $\delta_{RT}(t_{ref})$ is calculated. Inset: Plot of relaxation rate β as a function of $\delta_{RT}(t_{ref})$ for all the films.

slope $\beta = d\delta_{RT}/d[\log(t)]$ of such plots determines the relaxation rate. Since the current study concerns the relaxation in ambient conditions, β dictates the isothermal (at room temperature) and isobaric (at atmospheric pressure) relaxation of swollen polymer films. The first information that we can immediately draw from Figure 5 is that $\delta_{RT}(t)$ is greater for thinner films than for thicker ones and more importantly that the slope β follows the same trend. In addition, $\delta_{RT}(t)$ strongly depends on the depressurization rate as it can be seen for the slow depressurized 6.8 nm thick film which exhibits the same time evolution than the fast depressurized 21 nm thick film. As a general rule one can conclude that fast depressurized films show a much higher relaxation rate than the slow depressurized films.

In order to compare the values of δ_{RT} for (fast and slow depressurized) films of different thickness, we have chosen a reference time t_{ref} = 1 day. Actually, the comparison is made by plotting the values of β as a function of δ_{RT} at $t = t_{ref}$ (shown in the inset of Figure 5). It can be seen that the value of β which dictates the aging rate increases with $\delta_{RT}(t_{ref})$. An analogous behavior reported by Kovacs[58] and Richardson et al.[49] on thermal quenched polymers is a clear indication that the further the glassy polymer is away from its equilibrium, the faster it relaxes.

It is worth noting that the values of the relaxation rate ($\beta \sim 10^{-2}$–10^{-1}) observed here for the scCO$_2$ quenched ultrathin PS films is far higher than the one reported in other normal aging studies carried out on solvent quenched (freshly cast film) and temperature quenched PS,[47,48] PMMA,[49] and poly(isobutyl methacrylate (PiBMA)[59] films. Gray et al.[47] obtained $\beta \approx 9.5 \times 10^{-4}$ for ~400–1000 nm thick PS films at room temperature whereas Pye et al.[48] found $\beta \approx 10.5 \times 10^{-4}$

dx.doi.org/10.1021/ma501281t | Macromolecules XXXX, XXX, XXX–XXX

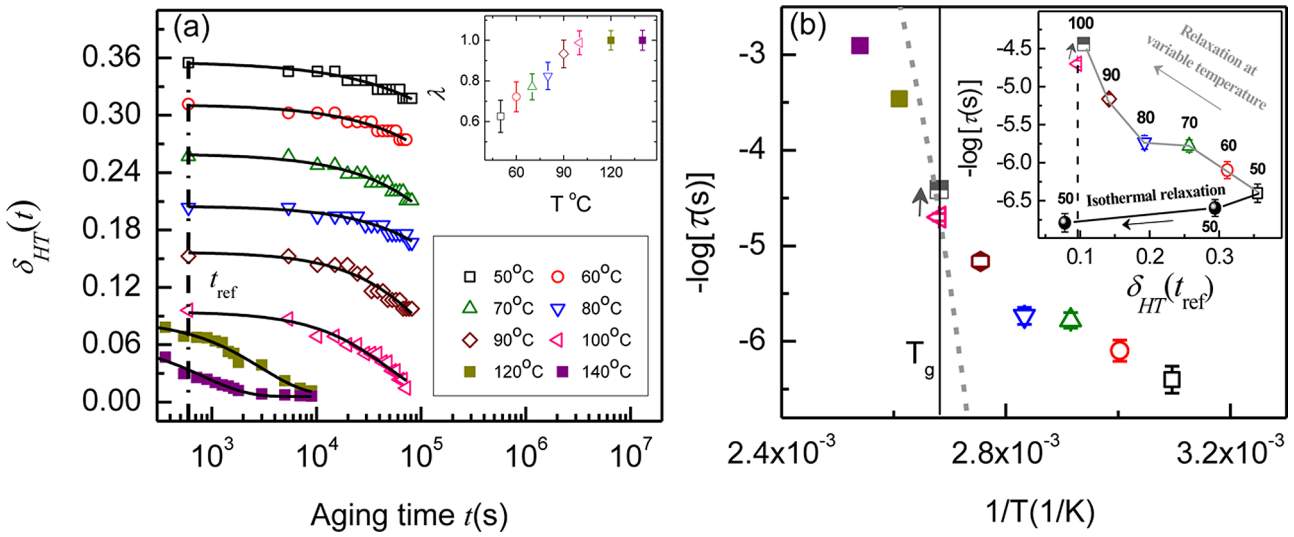

Figure 6. (a) Relaxation of 10.5 nm PS swollen film (open symbols) at high temperatures (up to 100 °C) after prolonged aging at room temperature (shown in Figure 3b and 5). Solid square symbols at 120 and 140 °C belong to two other swollen samples. Solid curves through symbols correspond to a fit using KWW equation (eq 2). The reference time t_{ref} (dashed line) is chosen to be $t_{ref} = 6 \times 10^2$ s. Inset: Plot of extracted λ values as a function of temperature T. (b) Temperature dependence of relaxation time constant τ (shown by symbols) below and above bulk T_g. Open symbols obtained from the successive measurements at different temperature starting from 50 to 100 °C on a single swollen film (10.5 nm). Two solid square symbols are obtained from two different films which having similar δ_{HT} around 0.06 ± 0.02. The arrow directed toward half-filled square (from triangle) at T_g (also in the inset) indicates the decrement in τ with the increase of δ_{HT}. The dashed curve obtained using WLF equation (eq 3) governs the α-relaxation in rubbery phase. Inset: corresponding plot of relaxation times vs $\delta_{HT}(t_{ref})$ that illustrates much more pronounced temperature-dependency behavior of τ than the δ_{HT}-dependency. The number next to each symbol indicates the temperatures of measurements.

and ≈7.7 × 10^{-4} for 2300 and 29 nm thick PS films respectively, at 338 K. Richardson et al.[49] reported $\beta \approx 2.5 \times 10^{-2}$ at 328 K for a 150 nm thick freshly cast PMMA film. They evidenced very small aging as the departure from the equilibrium state was small (≤10%). In our case the $scCO_2$ quenched 6.5 and 10.5 nm films exhibit a much higher relaxation of about 27% and 17%, respectively at similar aging conditions. Other films like the 14.5, 21, and 6.8 nm (slow) thick films show smaller relaxation (≤10%). However, the disparity in β can be attributed to the large influence of $scCO_2$ in the enlargement of existing free volumes and formation of new holes for thinner and fast depressurized films.

Temperature Dependence Study. Annealing at temperatures (50 °C ≤ T ≤ 100 °C) accelerates the relaxation and films recover their initial thicknesses and densities in a shorter time (see Supporting Information, Figure S2). This result is reminiscent of those obtained by Oka et al.[52] using PAS technique concerning the evolution of free volume of PS films exposed to $scCO_2$. The concept that aging is thermoreversible with small strains induced by cooling below T_g was already reported by Struik.[60] In the present work, we have monitored the evolution of film thickness at different temperatures as a function of time in order to obtain relaxation functions at each temperature. Figure 6a shows the evolution of δ_{HT} as a function of aging time t at HT starting from 50 to 100 °C for the 10.5 nm film and additionally at above T_g (up to 140 °C) for two other swollen films. In these variable-temperature measurements, δ_{HT} takes into account the fact that H_∞ increases with temperature due to the thermal expansion. For instance, H_∞ = 10.7 nm at 50 °C and 11.0 nm at 100 °C according to the thermal expansion coefficients provided by Ata et al.[54] In the contrary to the relaxation at room temperature (δ_{RT}), the relaxation observed at high temperatures (δ_{HT}) is not linear with logarithmic time scale (Figure 6a) but can be rather well explained by the Kohlrausch–Williams–Watts (KWW) equation[61,62] dealing with relaxation dynamics of polymers. The solid curves correspond to fits using KWW equation,

$$\delta_{HT}(t) = A\exp\left[-\left(\frac{t}{\tau}\right)^{\lambda}\right] \quad (2)$$

where τ and λ are known as KWW parameters which represent the relaxation time constants and stretched exponent, respectively. A is a constant. λ becomes 1 for single relaxation time, while deviation from 1 indicates the distribution of relaxation time. In fitting procedure A, τ, and λ are the fitting parameters. It is thus possible to extract from the fits the evolution of these parameters as a function of temperature. The temperature dependence of λ was found to increase monotonically with increasing temperature with a trend to reach λ = 1 above T_g [inset of Figure 6a]. This suggests a single relaxation time near T_g probably corresponds to dominant α-process (a cooperative segmental motion in which a large portion of the molecule move around) whereas at lower temperatures a distribution of relaxation times dictates the simultaneous occurring of β- (a local segmental motion due to thermal atomic motion) and the α-processes.

Let us now focus on the temperature dependence of τ which may provide essential information regarding the relaxation dynamics of polymer. As τ is fitted at different temperatures during the relaxation of the film, one can plot its temperature dependence (as shown in Figure 6b) as a function of $1/T$. It is striking to observe that $\tau(T)$ exhibits two different behaviors depending on whether the measurements are made below or above T_g. Below T_g, the behavior is obviously of the Arrhenius type (open symbols) while above T_g, a clear deviation (solid squares) from Arrhenius law is observed. This change can be interpreted by the dominant α-relaxation associated with the phase transition from the glassy to the rubbery state of PS. Indeed it is expected that $\tau(T)$ should strongly decrease above

dx.doi.org/10.1021/ma501281t | Macromolecules XXXX, XXX, XXX–XXX

T_g since the mobility of the chains is higher in the rubbery state. Actually τ is a function of both temperature and fractional free volume which is equivalent to the relative departure from equilibrium δ_{HT}.[63] The relative importance of these two parameters has been a controversial issue for many years since temperature variation necessarily induces a change in the free volume.[64] Our results provide some way to discriminate between these two parameters. The plot shown in the inset of Figure 6b illustrates this point. This plot gathers the results of two separate experiments: the first one concerns the measurement of δ_{HT} at a constant temperature of 50 °C (solid circles) on films of different thicknesses while the second one was made on the single film (10.5 nm) relaxed at variable temperatures (open symbols). For an isothermal relaxation one can see that τ does not change much though δ_{HT} strongly varies. On the contrary, τ changes by almost 2 orders of magnitude for the film studied from 50 to 100 °C within the same range of δ_{HT}. To illustrate the difference one can see that at a given value of δ_{HT} = 0.09 (dashed line in the inset of Figure 6b), log(τ) goes from 4.7 at 100 °C to 6.8 at 50 °C. As a conclusion one clearly stress that τ mainly depends on the temperature rather than on the change in free volume otherwise τ would not decrease with the decrease of δ_{HT} in a single film (open symbols) under variable-temperature measurements. On the other hand, it is striking to observe that τ considerably decreases with small increase in δ_{HT} at 100 °C (shown by small arrows at T_g). This trend predicts that at elevated temperatures (e.g., at 100 °C) the sensitivity of τ to δ_{HT} is stronger than at low temperatures (e.g., at 50 °C). However, we need further studies to explore the general behavior of relaxation as a function of δ_{HT} and T.

Above T_g, $\tau(T)$ can be modeled by the Williams, Landel, and Ferry (WLF) equation (dashed line in Figure 6b):[63−66]

$$\log \tau(T) = \log \tau(T_g) - \frac{C_1(T - T_g)}{C_2 + T - T_g} \quad (3)$$

where C_1 = 12.7, C_2 = 49.9, and $\tau(T_g) = 3 \times 10^4$ s is the relaxation time at T_g. The value of these parameters was obtained from literature[66] except the value of $\tau(T_g)$. The value of $\tau(T_g)$ obtained from the analysis of our relaxation data at the bulk T_g is 2 orders of magnitude higher than that of observed by other groups for PS bulk.[63] This difference can be attributed to the use of different probing techniques. The most common techniques used for studying relaxation dynamics are second harmonic generation (SHG)[63] and dielectric relaxation[67] which probe rotation and reorientation dynamics and can monitor dynamics from 10^{-4} s[68] to a very long time.[68] In that case chromophores are doped in nonpolar polymer like PS and in the presence of external electric field they attain a steady state. Withdrawing the field randomization of chromophore orientation in all the direction continues to occur with time. In contrast, XRR can only monitor the slow dynamics of evolution of film thickness in out-of-plane direction at the minute time scale. The rapid changes (~few seconds or subseconds) that occur during rotation and reorientation may not be immediately reflected in the effective change of overall film thickness measured by XRR. Hence a time lag may appear in the relaxation dynamics probed by different techniques. However, below T_g, the WLF curve does not agree with the observed data (see Figure 6b) as WLF theory is only applicable in the rubbery state. In the glassy state, the film is in a nonequilibrium state which contains higher free volume and accordingly a faster relaxation (i.e., lower τ) than those of the theoretical equilibrium state (continuation of WLF curve below T_g is shown by dashed curve in Figure 6b). Despite the fact that the WLF equation is valid above T_g, our data does not perfectly match with this equation (considering the parameters reported in case of bulk PS) probably because we are following the relaxation of polymer chains via the evolution of the overall film thickness rather than by measuring the much faster rotational or reorientation dynamics as mentioned before.

Mechanism of Swelling and Correlation with Relaxation. During the pressurization inside the $scCO_2$ cell, pressure and temperature are maintained at 80 bar and 35 °C respectively. This pressure is much higher than the glass transition pressure P_g at 35 °C (P_g ~ 20 and 40 bar for 7 and 17.5 nm PS films, respectively).[33] Thus, even though at T = 35 °C, PS remaining in the rubbery state under such conditions. During depressurization, pressure goes below P_g and PS is expected to come back to its glassy state (schematically depicted in Figure 7). For fast depressurization, pressure suddenly goes from 80 bar to below P_g and films become frozen in an expanded state which is likely associated with the temporally trapping of CO_2 molecules inside the film. Note that the presence of CO_2 molecules inside thin films has not yet been evidenced by direct methods such as Raman spectroscopy or infra-red spectroscopies due to the extremely small thickness of the films. For thicker films, the trapping of CO_2 in PS after depressurization was evidenced recently by Oka et al.[52] with weight measurements. This suggests that such a trapping is also possible for thinner films. Furthermore, as previously reported,[33] a hysteresis loop of the swellability during the in situ cycle appears between the pressurization and the depressurization steps as schematically shown in Figure 7. As glasses are usually described as systems that are far from equilibrium, the hysteresis may reveal that PS at a given pressure is further away from equilibrium during the depressurization than during the pressurization cycle due to the high swelling and high absorbed quantity of CO_2 in the supercritical state. During the depressurization, a continuous desorption of CO_2 takes place until the cell is brought back to atmospheric pressure. Hence, relaxation of polymer chains, which is evidenced by the thinning of film thickness, starts within the cell during depressurization.[33] Notably thinner films, such as 6.5 nm film, show higher density (~10%) in

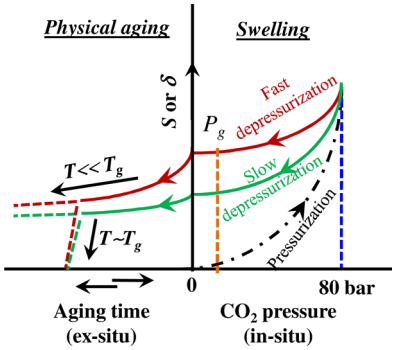

Figure 7. Schematic illustration of swellability S or relative departure from equilibrium δ (in situ and ex situ) and physical aging of swollen film in case of fast and slow depressurized films of similar thicknesses. Exposition is done at 80 bar and at 35 °C during 1 h in each case. P_g is the glass transition pressure at a particular temperature, say 35 °C. Physical aging strongly depends on aging temperature; it is faster when the temperature T is near to T_g than far below T_g.

dx.doi.org/10.1021/ma501281t | Macromolecules XXXX, XXX, XXX−XXX

comparison with thicker ones (21 nm). This higher density can be attributed to the fact that thinner films possess less free volume compared to thicker films. Recently[69] in contrast to the bulk density, we observed a ∼ 30% rise in density of 6 nm film (annealed at 160 °C during 24 h) on oxide-free (HF-treated) Si. This discrepancy can be ascribed to the annealing effect and probably the nature of the substrates. Furthermore, using variable energy positron annihilation lifetime spectroscopy (EVPALS) Ata et al.[70] reported that the free volume of thinner film (∼22 nm) is smaller than thicker one (∼1200 nm). As the density of thin film is correlated to its free volume, this clearly suggests that the thinner films should be denser than the thicker films under normal conditions of temperature and pressure. It is remarkable to observe that electron density after CO_2 exposure is constant ($\rho \approx 0.286$ e·Å^{-3}) whatever the initial thickness. This suggests that the mass density of the film before CO_2 exposure determines the swelling after CO_2 exposure.

Because of the finite rate of depressurization polymers remain in nonequilibrium swollen state of high energy instead of having their equilibrium state. Accordingly thermodynamic quantities, such as specific volume, entropy, and enthalpy are in higher energy states than in their corresponding equilibrium state at that particular temperature. Although molecular motion is greatly inhibited in the glassy state, some remaining finite motion allows such excess thermodynamic quantities to decrease toward equilibrium through physical aging process (schematically illustrated in Figure 7). In the present work, the relaxation that occurs in polymers which have undergone a large stress due to the drastic swelling upon absorption of CO_2 molecules within the polymer chains is studied rather than the one resulting from a thermal quench through the glass transition. Since the relaxation rate is known to be influenced by the segmental mobility of polymer chains, our measurements of the relaxation rate of swollen ultrathin films exposed to $scCO_2$ provide a way of probing molecular mobility in largely confined systems. A special issue is to find out how chains approach their equilibrium state from different out of equilibrium positions. The relaxation at room temperature is quite fast at the beginning but slows down with time when the chains are approaching their stable configuration. This accounts for the logarithmic decay of the overall thickness with aging time at room temperature. Therefore, in this case it is quite reasonable to consider that the initial relaxation of polymer chains is associated with the rapid release of trapped CO_2. According to the study of Oka et al.,[52] the swollen thick film (thickness ∼1 mm) takes 40−50 h to dry out after $scCO_2$ exposure although the relaxation of free volume continues further for a longer period of time. Thus, they concluded that during the initial stage i.e. for 50 h, the relaxation of free volume is accompanied by both the release of trapped CO_2 and the structural relaxation of polymer chains. After this duration, only the latter one continues. Thus, the release is probably taking place initially within the first few days. In the later stages, i.e., after a few days of depressurization, the aging at room temperature and then at higher temperatures is only associated with free volume relaxation which probably accounts for the logarithmic and KWW aging behavior, respectively. Such relaxations are accelerated upon increasing the temperature near T_g by providing excess thermodynamical driving force for relaxation (schematically shown in Figure 7, Figure 6a, and Supporting Information Figure S2).

CONCLUSION

XRR measurements were carried out to first investigate the swelling of PS ultrathin films exposed to $scCO_2$ and second to monitor their physical aging after they were brought back to ambient pressure. Fast depressurization leads to higher swollen film than slow depressurization. The thinner the films, the larger the swellability provided that the rate of depressurization is constant. Consequently physical aging of thin films was also more prominent than the one of thicker films. A detailed analysis of the physical parameters that are associated with the aging of the films is then presented. In particular we show how the thickness relaxation rate β is affected by the rate of depressurization and by the initial thickness of the film. We evidence that fast depressurization forces the films to be into an out of equilibrium state resulting in large β and small relaxation time τ whereas slow depressurization yields films close to their initial equilibrium state. We can thus tune the swelling/swellability and the stability of the PS films not only by varying the pressure within the cell but also by varying the depressurization rate or time.

In addition, the role of temperature on the aging of these swollen films was analyzed. We clearly evidence that the relaxation follows an Arrhenius law when films are kept below the bulk T_g while a departure from this behavior is seen above T_g. A model based on the WLF equation was tentatively used to explain the behavior above T_g. With the values reported for bulk PS in the literature, we fail to match the observed data, perhaps because the thickness-relaxation dynamics cannot keep pace with changes in the rotational or reorientation dynamics governing WLF behavior. Nonetheless, the trend suggested by this equation is confirmed. This study provides important information regarding the long-term stability of $scCO_2$-induced swollen PS films which may be useful in the design and manufacturing of polymers via nanofoaming, especially if their applications are to be at the temperatures below their T_g's.

ASSOCIATED CONTENT

Supporting Information

Swelling and physical aging of PS ultrathin film and relaxation of a swollen ultrathin PS film.This material is available free of charge via the Internet at http://pubs.acs.org.

AUTHOR INFORMATION

Corresponding Authors

*(A.G.): gibaud@univ-lemans.fr.
*(J.K.B.): jayanta.bal@gmail.com.

Notes

The authors declare no competing financial interest.

ACKNOWLEDGMENTS

This work was made possible thanks to the funding by the Région des Pays de la Loire of a postdoc grant to J.K.B. and to a Ph.D. grant to M.S.C. for whom the Région Bretagne is also funding half of the work. This work was made within the framework of the CEFIPRA program, for which we also acknowledge financial support. J.K.B thankfully acknowledged to Department of Science and Technology (DST), Government of India, for providing research grant through INSPIRE Faculty Award (IFA13-PH-79). The authors would like to acknowledge Frederic Amiard for his help in XRR instrumentation.

REFERENCES

(1) Bruno, T. J.; Ely, J. F. *Supercritical Fluid Technology: Reviews in Modern Theory and Applications*; CRC Press: Boston, MA, 1991.
(2) Cooper, A. I.; DeSimone, J. M. *Curr. Opin. Solid State Mater. Sci.* **1996**, *1*, 761−766.
(3) Kazarian, S. G. *Polym. Sci., Ser. C* **2000**, *42*, 78−101.
(4) DeSimone, J. M. *Science* **2002**, *297*, 799−803.
(5) McHugh, M. A.; Krukonis, V. *Supercritical Fluids Extraction Principles and Practice*; Butterworth-Heinemann: Boston, MA, 1994.
(6) Tomasko, D. L.; Li, H.; Liu; Han, X.; Wingert, M. J.; Lee, L. J.; Koelling, K. W. *Ind. Eng. Chem. Res.* **2003**, *42*, 6431−6456.
(7) Kendall, J. L.; Canelas, D. A.; Young, J. L.; DeSimone, J. M. *Chem. Rev.* **1999**, *99*, 543−564.
(8) Subramanium, B.; Rajewski, R. A.; Snarely, K. *J. Pharm. Sci.* **1997**, *86*, 885−890.
(9) Quinn, E. L.; Jones, C. L. *Carbon Dioxide*; Reinhold: New York, 1936.
(10) Wissinger, R. G.; Paulaitis, M. E. *J. Polym. Sci., Polym. Phys. Ed.* **1987**, *25*, 2497−2510.
(11) Shim, J. J.; Johnston, K. P. *AIChE J.* **1989**, *35*, 1097−1106.
(12) Wissinger, R. G.; Pallaitis, M. E. *Ind. Eng. Chem. Res.* **1991**, *30*, 842−851.
(13) Briscoe, B. J.; Zakaria, S. J. *J. Polym. Sci., Polym. Phys.* **1991**, *29*, 989−999.
(14) Goel, S. K.; Beckman, E. J. *Polymer* **1993**, *34*, 1410−1417.
(15) Garg, A.; Gulari, E.; Manke, W. *Macromolecules* **1994**, *27*, 5643−5653.
(16) Zhang, Y.; Gangwani, K. K.; Lemert, R. M. *J. Supercrit. Fluids* **1997**, *11*, 115−134.
(17) Chang, S. H.; Park, S. C.; Shim, J. J. *J. Supercrit. Fluids* **1998**, *13*, 113−119.
(18) Royer, J. R.; DeSimone, J. M.; Khan, S. A. *Macromolecules* **1999**, *32*, 8965−8973.
(19) Horn, N. R.; Paul, D. R. *Macromolecules* **2012**, *45*, 2820−2834.
(20) Koga, T.; Seo, Y. S.; Zhang, Y.; Shin, K.; Kusano, K.; Nishikawa, K.; Rafailovich, M. H.; Sokolov, J. C.; Chu, B.; Peiffer, D.; Occhiogrosso, R.; Satija, S. K. *Phys. Rev. Lett.* **2002**, *89*, 125506−125509.
(21) Sirard, S. M.; Ziegler, K. J.; Sanchez, I. C.; Green, P. F.; Johnston, K. P. *Macromolecules* **2002**, *35*, 1928−1935.
(22) Sirard, S. M.; Gupta, R. R.; Russell, T. P.; Watkins, J. J.; Green, P. F.; Johnston, K. P. *Macromolecules* **2003**, *36*, 3365−3373.
(23) Pham, J. Q.; Sirard, S. M.; Johnston, K. P.; Green, P. F. *Phys. Rev. Lett.* **2003**, *91*, 175503−1−4.
(24) Koga, T.; Seo, Y. S.; Shin, K.; Zhang, Y.; Rafailovich, M. H.; Sokolov, J. C.; Chu, B.; Satija, S. K. *Macromolecules* **2003**, *36*, 5236−5243.
(25) Gupta, R. R.; Lavery, K. A.; Francis, T. J.; Webster, J. R. P.; Smith, G. S.; Russell, T. P.; Watkins, J. J. *Macromolecules* **2003**, *36*, 346−352.
(26) Pham, J. Q.; Johnston, K. P.; Green, P. F. J. *Phys. Chem. B* **2004**, *108*, 3457−3461.
(27) Meli, L.; Pham, J. Q.; Johnston, K. P.; Green, P. F. *Phys. Rev. E* **2004**, *69*, 051601−1−8.
(28) Koga, T.; Ji, Y.; Seo, Y. S.; Gordon, C.; Qu, F.; Rafailovich, M. H.; Sokolov, J. C.; Satija, S. K. *J. Polym. Sci., Part B: Polym. Phys.* **2004**, *42*, 3282−3289.
(29) Cao, T.; Johnston, K. P.; Webber, S. E. *Macromolecules* **2005**, *38*, 1335−1340.
(30) Koga, T.; Akashige, E.; Reinstein, A.; Bronner, M.; Seo, Y. S.; Shin, K.; Rafailovich, M. H.; Sokolov, J. C.; Chu, B.; Satija, S. K. *Physica B* **2005**, *357*, 73−79.
(31) Li, Y.; Park, E.; Lim, K.; Johnston, K. P.; Green, P. F. *J. Polym. Sci., Part B: Polym. Phys.* **2007**, *45*, 1313−1324.
(32) Koga, T.; Gin, P.; Yamaguchi, H.; Endoh, M. K.; Asada, M.; Sendogdular, L.; Kobayashi, M.; Takahara, A.; Akgun, B.; Satija, S. K.; Sumi, T. *Polymer* **2011**, *52*, 4331−4336.
(33) Chebil, M. S.; Vignaud, G.; Grohens, Y.; Konovalov, O.; Sanyal, M. K.; Beuvier, T.; Gibaud, A. *Macromolecules* **2012**, *45*, 6611−6617.
(34) Keddie, J. L.; Jones, R.; Cory, R. *Faraday Discuss.* **1994**, *98*, 219−230.
(35) Frank, C. W.; Rao, V.; Despotopoulou, M. M.; Pease, R. F. W.; Hinsberg, W. D.; Miller, R. D.; Rabolt, J. F. *Science* **1996**, *272*, 912−915.
(36) Rivillon, S.; Auroy, P.; Deloche, B. *Phys. Rev. Lett.* **2000**, *84*, 499−502.
(37) Frank, B.; Gast, A. P.; Russell, T. P.; Brown, H. R.; Hawker, C. *Macromolecules* **1996**, *29*, 6531−6534.
(38) Benkoski, J. J.; Fredrickson, G. H.; Kramer, E. J. *J. Polym. Sci., Part B: Polym. Phys.* **2002**, *40*, 2377−2386.
(39) Besancon, B. M.; Soles, C. L.; Green, P. F. *Phys. Rev. Lett.* **2006**, *97*, 057801−1−4.
(40) Bodycomb, J.; Funaki, Y.; Kimishima, K.; Hashimoto, T. *Macromolecules* **1999**, *32*, 2075−2077.
(41) Fleming, G. K.; Koros, W. J. *Macromolecules* **1986**, *19*, 2285−2291.
(42) Sirard, S. M.; Green, P. F.; Johnston, K. P. *J. Phys. Chem. B* **2001**, *105*, 766−772.
(43) Fishburn, G. D. *Adsorption of Poly(dimethylsiloxane) from Supercritical Carbon Dioxide*. Thesis. University of Massachusetts—Amherst: Amherst, MA, 1999.
(44) Gibaud, A.; Vignaud, G. In *X-ray and Neutron Reflectivity*; Daillant, J., Gibaud, A., Eds.; Springer: Berlin, Germany, 2009, Lecture Notes in Physics 770, pp 85−131.
(45) Gibaud, A.; Chebil, M. S.; Beuvier, T. Chapter 7 in *Surface Science Techniques*, Eds. Bracco, G.; Holst, B. Springer: Verlag: Berlin Heidelberg, 2013.
(46) Bal, J. K.; Mukherjee, M.; Delorme, N.; Sanyal, M. K.; Gibaud, A. *Langmuir* **2014**, *30*, 5808−5816.
(47) Gray, L. A. G.; Yoon, S. K.; Pahner, W. A.; Davidheiser, J. E.; Roth, C. B. *Macromolecules* **2012**, *45*, 1701−1709.
(48) Pye, J. E.; Rohald, K. A.; Baker, E. A.; Roth, C. B. *Macromolecules* **2010**, *43*, 8296−8303.
(49) Richardson, H.; López-García, Í.; Sferrazza, M.; Keddie, J. L. *Phys. Rev. E* **2004**, *70*, 051805−1−8.
(50) Bos, A.; Pünt, I. G. M.; Wessling, M.; Strathmann, H. *J. Membr. Sci.* **1999**, *155*, 67−78.
(51) Chiou, J. S.; Barlow, J. W.; Paul, D. R. *J. Appl. Polym. Sci.* **1985**, *30*, 2633−2642.
(52) Oka, T.; Ito, K.; He, C.; Dutriez, C.; Yokoyama, H.; Kobayashi, Y. *J. Phys. Chem. B* **2008**, *112*, 12191−12194.
(53) Chen, H.; Cheng, M.; Jean, Y. C.; Lee, L. J.; Yang, J. *J. Polym. Sci., Part B: Polym. Phys.* **2008**, *46*, 388−405.
(54) Ata, S.; Muramatsu, M.; Takeda, J.; Ohdaira, T.; Suzuki, R.; Itob, K.; Kobayashi, Y.; Ougizawa, T. *Polymer* **2009**, *50*, 3343−3346.
(55) Koga, T.; Seo, Y.-S.; Zhang, Y.; Shin, K.; Kusano, K.; Nishikawa, K.; Rafailovich, M. H.; Sokolov, J. C.; Chu, B.; Peiffer, D.; Occhiogrosso, R.; Satija, S. K. *Phys. Rev. Lett.* **2002**, *89*, 125506−1−4.
(56) Sirard, S. M.; Ziegler, K. J.; Sanchez, I. C.; Green, P. F.; Johnston, K. P. *Macromolecules* **2002**, *43*, 1928−1935.
(57) Kurchan, J. *Nature* **2005**, *433*, 222−225.
(58) Kovacs, A. J. *Forschr. Hochpolym.-Forsch.* **1964**, *3*, 394−507.
(59) Ellison, C. J.; Kim, S. D.; Hall, D. B.; Torkelson, J. M. *Eur. Phys. J. E* **2002**, *8*, 155−166.
(60) Struik, L. C. E. *Polym. Eng. Sci.* **1977**, *17*, 165−173.
(61) Kohlrausch. *Ann. Phys. (Leipzig)* **1847**, *12*, 393−401.
(62) Williams, G.; Watts, D. C. *Trans. Faraday Soc.* **1970**, *66*, 80−85.
(63) Dhinojwala, A.; Wong, G. K.; Torkelson, J. M. *J. Chem. Phys.* **1994**, *100*, 6046−6054.
(64) Mark, J. E. *Physical Properties of Polymer Handbook*; Springer: New York, 2007.
(65) Williams, M. L.; Landel, R. F.; Ferry, J. D. *J. Am. Chem. Soc.* **1955**, *77*, 3701−3707.
(66) Fakhraai, Z.; Forrest, J. A. *Science* **2009**, *319*, 600−604.
(67) Schlosser, E.; Schonhals, A. *Polymer* **1991**, *32*, 2135−2140.
(68) Dhinojwala, A.; Wong, G. K.; Torkelson, J. M. *Macromolecules* **1993**, *26*, 5943−5953.

(69) Vignaud, G.; Chebil, M. S.; Bal, J. K.; Delorme, N.; Beuvier, T.; Grohens, Y.; Gibaud, A. *Langmuir* **2014**, *30*, 11599−11608.
(70) Ata, S.; Muramatsu, M.; Takeda, J.; Ohdaira, T.; Suzuki, R.; Ito, K.; Kobayashi, Y.; Ougizawa, T. *Polymer* **2009**, *50*, 3343−3346.